2.B Diagnostic Value of Odd-Integer Half-Harmonic Spectra

UV-laser/plasma interaction experiments carried out recently at LLE have significantly extended our understanding of the nonlinear coupling of laser light to the coronal plasma. One of the most important of these parametric processes is the $2\omega_p$ decay instability at the quarter-critical density ($n_c/4$). The signature of this process encompasses a broad spectral band of electromagnetic radiation from $\approx$ 1 eV to several keV. The behavior of structural features in the $\omega_0/2$ and $3\omega_0/2$ spectra reveals a great deal about the internal coronal processes. In particular, some of the features are especially suitable for coronal-electron-temperature diagnostics.

Odd-integer half-harmonic spectra have been observed and reported in the literature since 1970.[1] The connection of these spectra with instabilities occurring in the plasma corona near $n_c/4$ is now clearly established. As such, these spectra can serve as a qualitative diagnostic for the existence of these instabilities, but, in addition, various theoretical predictions[2] have been made for the spectral splitting of the observed, generally double-peaked, spectra. All theories predict a linear relationship between splitting and coronal electron temperature, hence the interest in using these spectra as a coronal-temperature diagnostic. Unfortunately, the spectral splitting generally also depends on geometrical factors such as the angles of incidence and the angles of observation in addition to other effects.[3,4] Since these conditions are usually not very well defined — they typically differ from experiment to experiment — the diagnostic value of these spectra rapidly diminishes as a quantitative analysis requires complex geometrical and other factors to be included.

Recent advances in the understanding of the half-harmonic spectra[5] from spherical UV target-irradiation experiments on the OMEGA laser system have isolated one feature in the half-harmonic spectra which appears to follow a simple relationship between the temperature and its frequency shift from $\omega_0/2$ (ω_0 = irradiation frequency). This shift is independent of detailed geometrical or other effects. However, this feature — a sharp, slightly red-shifted spike — can generally only be seen when viewing the plasma along or close to the density gradient. This particular feature thus represents a convenient diagnostic for the determination of the coronal electron temperature.

The other features in the half-harmonic and the three-halves-harmonic spectra have traditionally been interpreted in various ways although their complex dependences on angles of incidence and angles of observation render them practically useless for temperature diagnostics. In this article we will discuss the various spectral features of the odd-integer half-harmonics, their interpretation, and their diagnostic value for laser plasmas.

A schematic diagram of the irradiation and observation configuration in the $\omega_0/2$ and $3\omega_0/2$ experiments on OMEGA is shown in

Fig. 19.5. One of the six UV beams of OMEGA (λ_L = 351 nm) is shown illuminating the target at an angle of 120° to the axis of the port of observation. If we assume that the plasma is roughly spherical, then the region on the target surface emitting $\omega_0/2$ light into the collection optics is restricted to less than 20° around the direction defined by the target center and the center of the collection optics. This is a result of the fact that the $\omega_0/2$ radiation originates very close to its own critical density; thus, it is refracted strongly and emerges close to the direction of the density gradient in the plasma. This also implies oblique angles of incidence for the other beams at 30° and 60° with respect to the observation port.

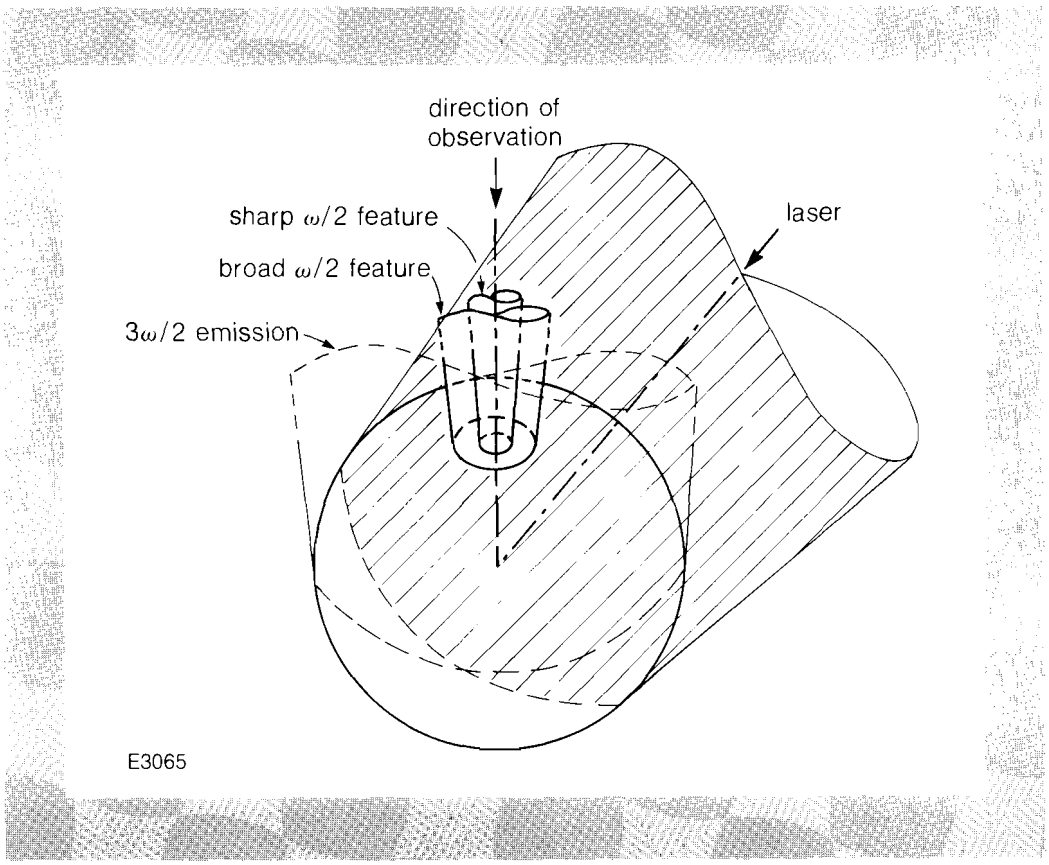

Fig. 19.5
Schematic diagram showing the OMEGA irradiation and observation configuration for the $\omega/2$ and $3\omega/2$ experiments. For clarity, only one laser beam is shown. (Typically, six overlapping beams illuminated the target.) For a particular direction of observation, the sharp $\omega_0/2$ feature is seen only in a small region about the normal to the target surface. The broad $3\omega_0/2$ radiation shows no such preferential direction of emission; thus, the entire hemisphere is visible in this region of the spectrum.

The evolution of half-harmonic spectra with increasing intensity and for different target materials (Z) is shown in Fig. 19.6. We note that only a sharp spike with near resolution-limited width is observed at the lowest intensities. With increasing intensity a clear, additional, spectrally broad, blue-shifted feature appears. A similar, spectrally broad, red-shifted feature of much less intensity also becomes apparent at higher intensities.

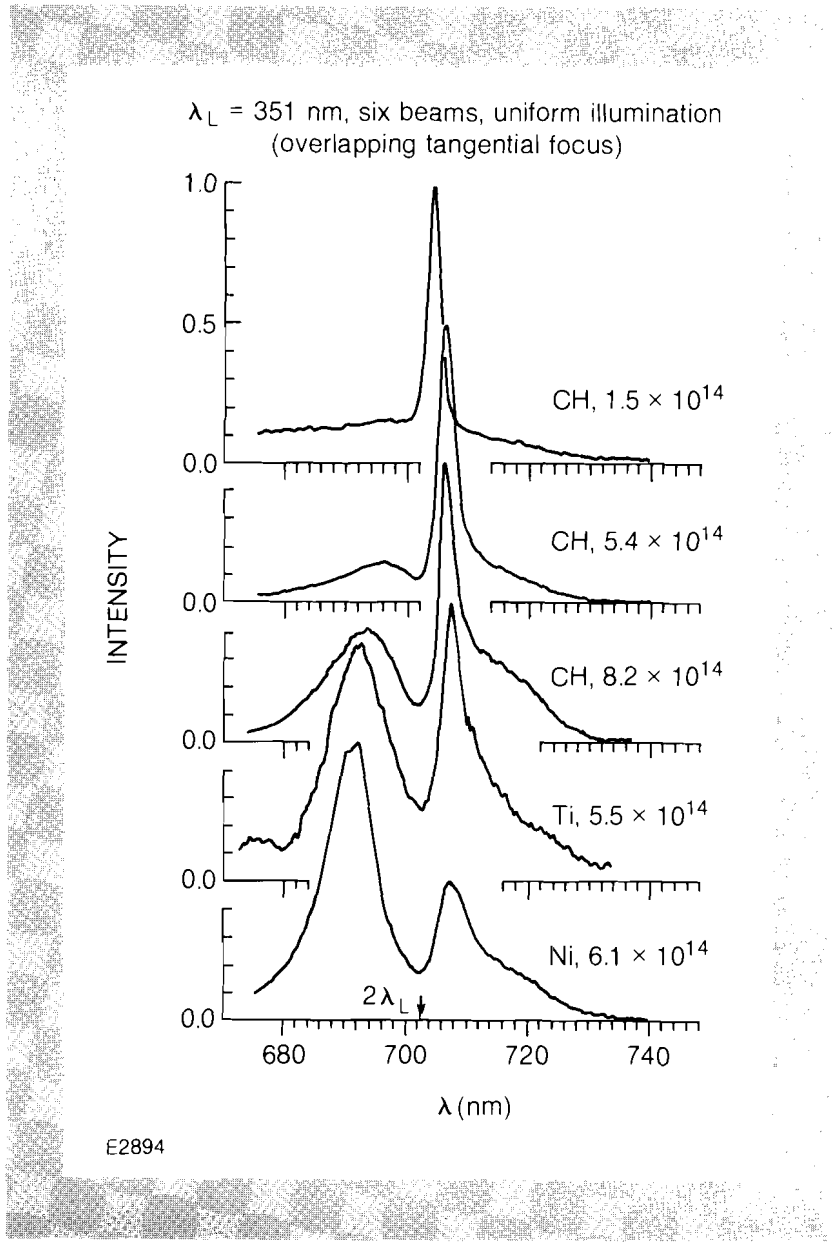

Fig. 19.6
Evolution of $\omega/2$ spectra from uniformly (tangentially) illuminated spherical targets for different irradiation intensities. The sharp, slightly red-shifted peak seen in all spectra can be effectively used for coronal-electron-temperature diagnosis.

In a previous report[5] we have shown a typical spectrum taken in the mid-10^{14} W/cm^2 range and have offered an interpretation in terms of ordinary Raman down-scattering for the sharp feature and in terms of plasmon-photon reconversion (inverse resonance absorption) for the two broad features. Recent theoretical work has strengthened this interpretation of the sharp component, while alternative explanations for the other features now appear more likely, as discussed below.

As the generation of half-harmonic light can involve either the $2\omega_p$-decay instability and/or the absolute stimulated Raman-scattering instability, we must consider the threshold conditions for these processes. Equation (1) shows the threshold relations including effects due to oblique incidence (θ is the internal angle of incidence at $n_c/4$).

$$I_{th}^{2\omega_p} \lambda^2 \left(\frac{L}{\lambda}\right) \frac{1}{T} \approx 7 \times 10^{15} \cos\theta \ (\mathrm{W}\,\mu\mathrm{m}^2/\mathrm{cm}^2\,\mathrm{keV})$$

$$I_{th}^{SRS} \lambda^2 \left(\frac{L}{\lambda}\right)^{4/3} \approx 10^{18} \ (\mathrm{W}\,\mu\mathrm{m}^2/\mathrm{cm}^2). \qquad (1)$$

Here, all intensities are in W/cm^2, the density scale lengths and laser wavelengths are in μm, and T_e is the coronal electron temperature in keV. Typical estimated plasma parameters for our experiments are $T_e \approx 1$ keV, $L \approx 20$-50 μm, $\theta \approx 60°$, and $\lambda_L = 0.35$ μm which lead to threshold intensities of $I_{th}^{SRS} \approx 5\times10^{15}$ W/cm^2 and $I_{th}^{2\omega_p} \approx 1.5\times10^{14}$ W/cm^2. For the range of irradiation intensities in our experiments, $10^{13} \lesssim I \lesssim 2\times10^{15}$ W/cm^2, we are clearly above the $2\omega_p$ instability threshold while we are well below the SRS threshold even after allowance is made for intensity nonuniformities on the target surface. On this basis we reject SRS as a contributing factor to our half-harmonic spectra and will concentrate in the following on the $2\omega_p$ decay instability as the main factor influencing the observed spectra.

In explaining the $\omega_o/2$ spectra it is necessary to refer to a typical $2\omega_p$-decay diagram as shown in Fig. 19.7. Here, the incident photon with frequency ω_o and wave vector k_o decays into two plasmons with $\omega_{p_{1,2}} = \omega_o/2 \pm \Delta\omega$ and $k_{p_{1,2}}$ as shown in the figure where the frequency shift is given by

$$\Delta\omega/\omega_o = 9/4\ \kappa\ (v_T^2 k_o^2/\omega_o^2) \approx 4.4 \cdot 10^{-3}\ \kappa\ T_{e(keV)}$$

and

$$\kappa = \mathbf{k}_{p_1} \cdot \mathbf{k}_o / k_o^2.$$

Fig. 19.7
Wave-vector diagrams for the $2\omega_p$-decay instability and for Raman down-scattering. The $2\omega_p$ diagrams are formed by $\mathbf{k}_o = \mathbf{k}_{p_1} + \mathbf{k}_{p_2}$ while the Raman scattering is given by $\mathbf{k}_s = \mathbf{k}_o - \mathbf{k}_p$. For normal incidence (a) the k-matching conditions for Raman scattering can only be satisfied for $k_s \approx 0$, while for oblique incidence the conditions can only be met for ∇n nearly parallel to $\mathbf{k}_p$.

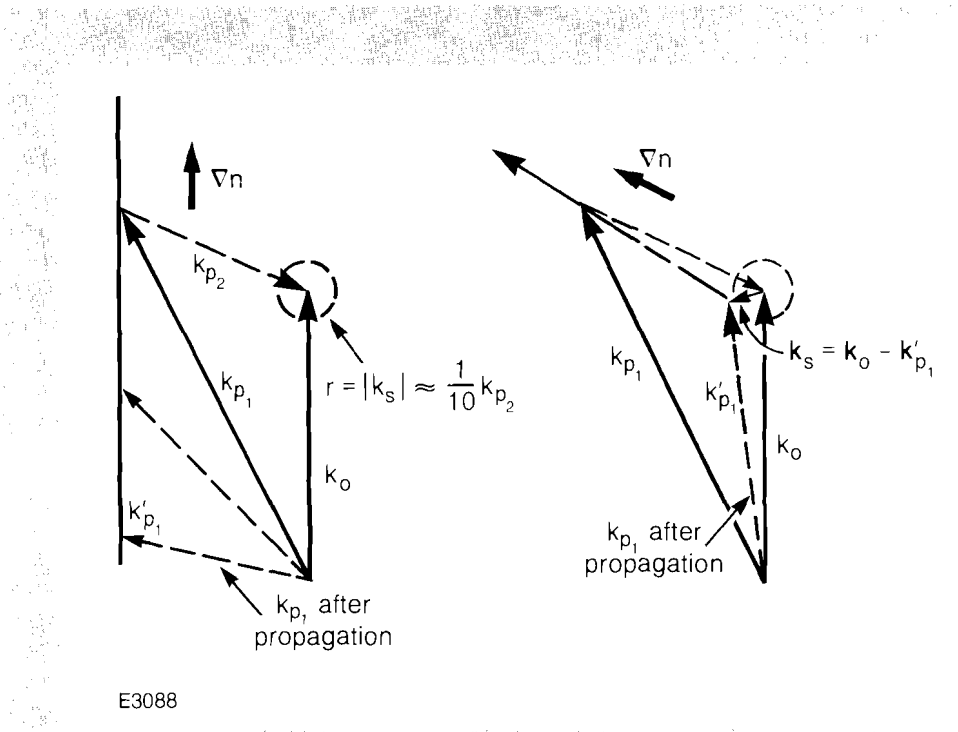

E3088

To generate $\omega_0/2$ light via Raman down-scattering of incident light from plasmons produced by the $2\omega_p$ instability, the Raman frequency and k-matching conditions have to be satisfied, i.e., $\omega_s = \omega_0 - \omega_p$, and $\mathbf{k}_s = \mathbf{k}_0 - \mathbf{k}_p$ (Fig. 19.7). Since the k-vector of the scattered EM wave, k_s, is approximately one-tenth the size of the plasmon k-vector of the same frequency, Raman down-scattering can happen only if one of the plasmon k-vectors is nearly zero or the density gradient is nearly aligned with one of the plasmons, or if the EM wave which scatters off the plasmon is not the same as the incident EM wave giving rise to the $2\omega_p$ decay. The usual theory[6] for the $2\omega_p$ decay instability does not include the mode for which one plasma k-vector is zero or nearly zero. However, recent analysis (theoretical work in progress[7]) indicates that there is indeed such a mode which is similar to, but not identical with, the usual absolute SRS instability.

This decay mode involves two waves — a plasma wave whose k-vector is very nearly equal to the pump-wave vector and a second wave which is a hybrid between an electromagnetic and electrostatic wave of near-zero k-vector. The hybrid wave is expected to radiate light efficiently at a frequency slightly less than $\omega_0/2$. On the basis of k-matching and growth rate considerations, we conclude that the spectrum of this emission is narrow as well as slightly red-shifted. This corresponds to the dominant feature in the spectra shown in Fig. 19.6.

The threshold for this mode is slightly higher than the ordinary $2\omega_p$ threshold, but since this mode is an efficient radiator of $\omega_0/2$ light it may well become visible before any other manifestation of the usual $2\omega_p$-decay instability.

The frequency shift of this narrow, red-shifted $\omega/2$ component is well defined ($\kappa = 1/2$) and given by $\Delta\omega/\omega_0 = 2.2\text{x}10^{-3}\ T_{e\ (\text{keV})}$. The width of this spectral feature is determined by the convolution of the growth rate for the primary decay process and the Raman k-matching conditions. Fortunately, the frequency shift of this mode is not affected by the irradiation or observation geometry. Thus, the sharp and slightly red-shifted half-harmonic spectral feature is a very good temperature diagnostic for the corona. As an application of these conclusions, we have plotted in Fig. 19.8 the intensity dependence of the frequency shift of the narrow, red-shifted component (closed symbols). On the right-hand ordinate the electron temperature scale is shown corresponding to the relationship

$$\Delta\omega/\omega_0 = 2.2 \cdot 10^{-3}\ T_{e\ (\text{keV})}.$$

The temperatures thus deduced are in close agreement with earlier work[8] where certain spectral features of the convective SRS emission were used as a coronal-temperature diagnostic. Hydrocode predictions for these plasmas typically lie 20-50% above measurements reported here. The origin of this discrepancy may lie in the thermal electron transport around the critical density n_c and is currently under active investigation.

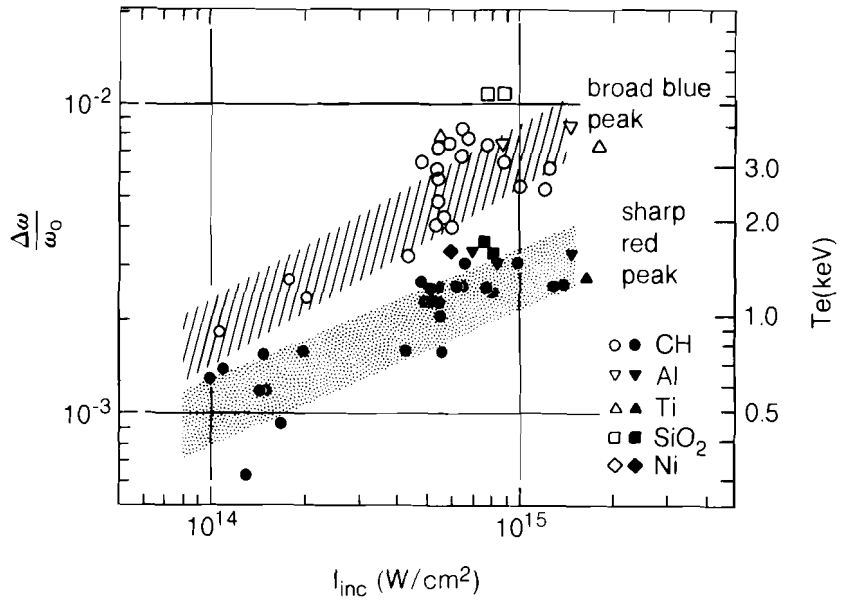

Fig. 19.8
Normalized frequency shifts of $\omega/2$ spectra for uniform (tangential), multi-beam irradiation of spherical targets (λ_L= 351 nm, t_L= 600 ps). The frequency shift of the sharp, red-shifted $\omega/2$ feature is shown in closed symbols. The interpretation of this shift in terms of electron temperature is shown on the right-hand ordinate using the relation $\Delta\omega/\omega_0=2.2\times10^{-3}\ T_e(keV)$. (Note that this temperature scale applies to the solid dots only.) The frequency shift of the broad blue component of the $\omega/2$ spectra is shown in open symbols.

The broad $\omega_0/2$ spectral features seen in Fig. 19.6 can be explained either by inverse resonance absorption (IRA) or Raman down-scattering. Analysis of the former shows that in a one-dimensional (1-D) spherical plasma the resulting spectra should be narrow and their shifts from $\omega_0/2$ should be much smaller than observed. Rippling of the $n_c/4$ density surface could broaden the spectrum, but it still appears that the large observed spectral shifts cannot be explained in this way. Thus, we rule out IRA as the process responsible for the broad features in the $\omega_0/2$ spectra.

Similarly, Raman down-scattering involving incident photons (k_0) and plasmons arising from decays with $k_{p_2} \neq 0$ encounters severe difficulties in satisfying the Raman k-matching conditions. However, Raman down-scattering can generate broad spectral features with the required shifts and widths if we allow the participating EM wave with frequency ω_0 to have a direction other than the incident photons. This process was recently proposed by Turner *et al.*[9] without, however, specifying any further conditions. They could, therefore, not predict any particular spectral shape or shift except for broadly bracketing the spectral range of the $\omega_0/2$ emission. However, we have found a special case of Raman down-scattering[10] which

involves a low frequency ("red") plasmon whose k-vector length is equal to the length of the incident EM wave vector. If we assume the existence of an EM wave with the fundamental frequency and with its wave vector aligned with that of the red plasmon, then the Raman down-scattering conditions are met exactly in the $2\omega_p$-decay region. The result is a blue-shifted $\omega_0/2$ spectral component whose estimated spectral shift and width agree closely with experimental measurements. We note that this is not a general result but one which is a direct consequence of requiring the particular $2\omega_p$ decay with $|k_{p_2}| \approx |k_0|$.

The theoretical analysis of this Raman down-scattering process further shows that the blue-shift of this component bears a nearly constant relationship to the frequency shift of the sharp red component, independent of geometry and intensity. That is, the two shifts differ by approximately a factor of 2. This conclusion also agrees closely with our observations, as is borne out in the intensity scaling of the frequency shifts of the two half-harmonic spectral features (open and closed symbols in Fig. 19.8). In this context it is also interesting to note that the data points for the blue peak set in at higher irradiation intensities than those for the red peak. This is also seen in Fig. 19.6, and finds its explanation in the higher thresholds for the $2\omega_p$ decays involving the long plasmon k-vectors necessary for the blue Raman down-scattering component.

Another consequence of this model is that the spectrally broad blue component is emitted into a much wider cone around the direction of the density gradient than the sharp red spike. This is due to the lengths of the scattered k-vectors k_s, which are essentially zero for the sharp red-shifted spike (the emission originates at its critical density) while for the spectrally broad blue-shifted component they are $|k_s| \approx 0.2|k_0|$. That is, the emission originates from a region with considerably less than its critical density. Viewed from outside the plasma, the cone angle for this emission can be estimated to be

$$\theta \approx \sin^{-1}\left(\frac{0.2 \times 0.87}{0.5}\right) \approx 20°.$$

This agrees closely with observations made here in our experiments as well as elsewhere,[9] in which the sharp, red-shifted component appears to emanate from a narrow coronal region. This region is centered about the normal to the target surface that passes through the observation point.

The origin of the EM waves (k_0', ω_0) which give rise to the blue-shifted Raman component may in our experiments come from one of the other six beams illuminating the target. In flat-target experiments as reported in Ref. 9, the scattered fundamental radiation could come from a rippled critical-density surface or from filamentation which had to be invoked for the interpretation of data obtained in such experiments.[2,11] Turner *et al.*[9] have suggested stimulated Brillouin scattering as an alternative source for the scattered light. We cannot rule out this source in our experiments although we have never observed evidence for stimulated Brillouin side-scattering.

The low-intensity, broad, red-shifted component in the half-harmonic spectra (Fig. 19.6) can be explained in a manner similar to the explanation for the blue component. Here, however, propagation of the high-frequency (blue) plasmon in the density gradient is required. Regarding spectral shifts and widths, the same arguments apply as delineated above, making this red feature symmetrical to the blue feature in all aspects except its intensity. The latter is expected to be lower because the blue plasmon must propagate approximately 1 μm in the density gradient before reaching the Raman k-matching point.

In short, the half-harmonic spectra now appear to be reasonably well understood, with one feature exhibiting a red-shift (sharp red spike) which is simply related to the coronal electron temperature. However, this feature is generally only observed when viewing the plasma close to the target normal (along the density gradient). The other prominent feature of the $\omega_0/2$ spectra is a broad blue component which is more easily observed (within $\approx 20°$ of the target normal) and whose blue-shift is roughly twice the frequency shift of the sharp red component. Although this proportionality is somewhat dependent on irradiation intensity and geometry, it is sufficiently close to make this spectral feature an alternate (though less desirable) candidate for coronal-temperature diagnostics. The third and much weaker component now appears to be understood the same way as the broad blue peak, but because of its weakness its diagnostic value is of minor importance.

The coronal-temperature diagnostic most frequently reported in the literature uses the splitting of the 3/2-harmonic spectra. The theories usually applied[2] predict symmetrically split spectra for normal incidence. All $3\omega_0/2$ light generated in the backward direction is red shifted, while the forward component is blue shifted with the shifts depending strongly on the angle of observation. For overdense targets this translates into symmetrically split spectra in the backscatter direction, but the detailed predictions of the 1-D theory have never been verified experimentally. Recent spectra taken with thin targets[3] have, however, shown interesting angular dependence of the emitted $3\omega_0/2$ spectra which could be understood in terms of filamentation of the incident laser light in the plasma. Since truly 1-D plasmas are extremely difficult to produce, most of the experimental spectra probably suffer from various two-dimensional (2-D) effects which can wash out the expected angular dependence of the spectral splitting. Under those conditions the average splitting is extremely difficult to predict, thereby reducing significantly the value of the 3/2-harmonic spectra as a coronal-electron-temperature diagnostic. Typically, the temperatures deduced from applying existing theories without geometrical correction factors lie two to three times above those which would be obtained from the half-harmonic spectra discussed above.

Typical 3/2-harmonic spectra obtained on OMEGA six-beam experiments are shown in Fig. 19.9 for nonuniform illumination of the targets. The poor reproducibility and irregularity of these spectra

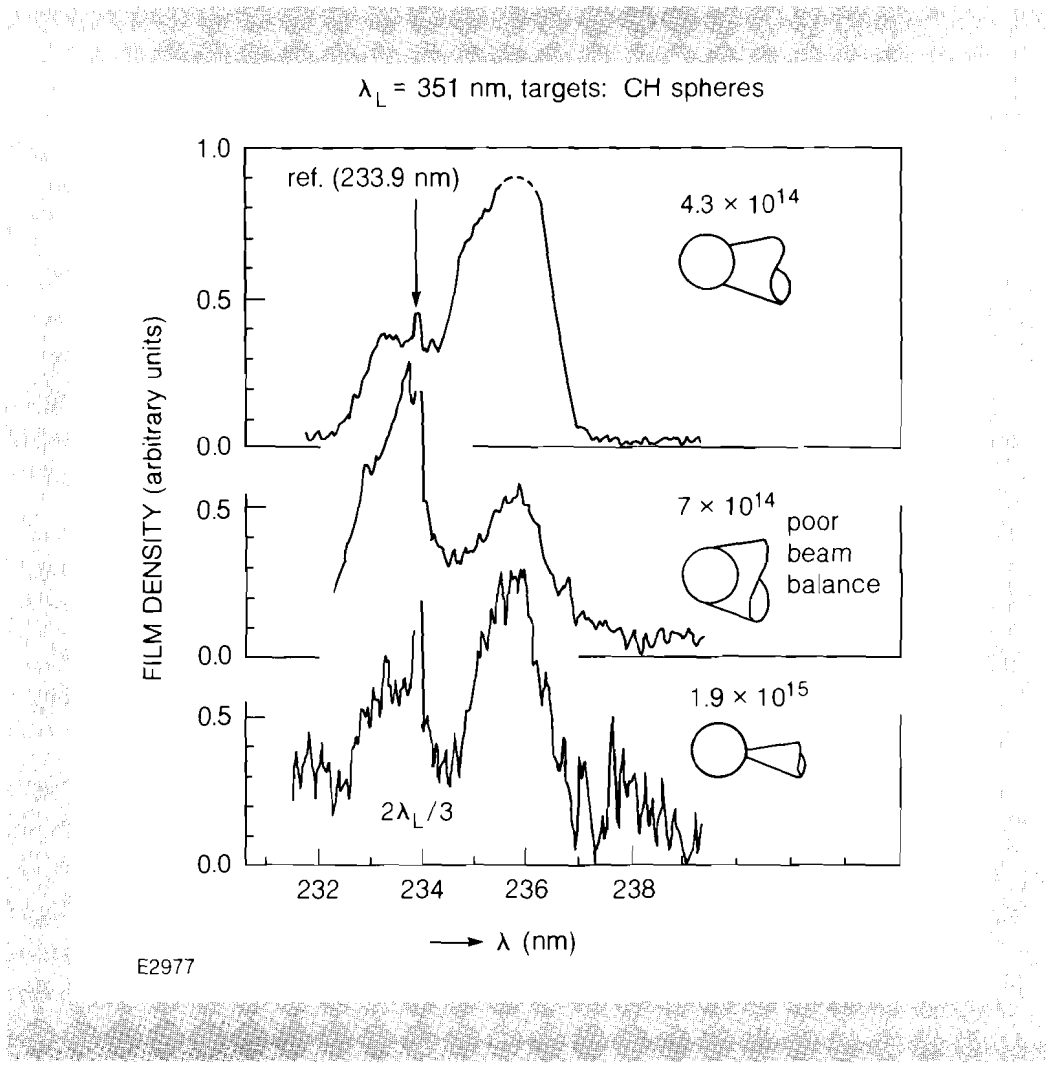

Fig. 19.9
Three-halves-harmonic spectra obtained on the six-UV-beam OMEGA system for nonuniform illumination of targets (focusing as indicated in the inserts). We note the strongly changing spectral features under these conditions which reflect the dependence of these spectra on irradiation and observation configuration.

underline the conclusions drawn above — that the 3/2-harmonic spectra are very sensitive to geometrical factors. The intensity dependence of the spectral splitting of the 3/2- and 1/2-harmonic spectra is shown in Fig. 19.10. For simplicity we have drawn half the spectral splitting of the $3\omega_0/2$ spectra along with the normalized frequency shift of the sharp red spike of the $\omega_0/2$ spectra. If the two processes were to sample the same plasmons, the two sets of data would lie on top of each other. It is evident from this figure that the intensity scaling is different for the two sets of data. Thus, we conclude that the 3/2-harmonic spectra hardly reflect any particular feature of the plasmon spectra produced by the $2\omega_p$-decay instability. The usefulness of the 3/2-harmonic spectra is therefore reduced to a qualitative answer to the questions of the existence of the $2\omega_p$-decay instability in the plasma.

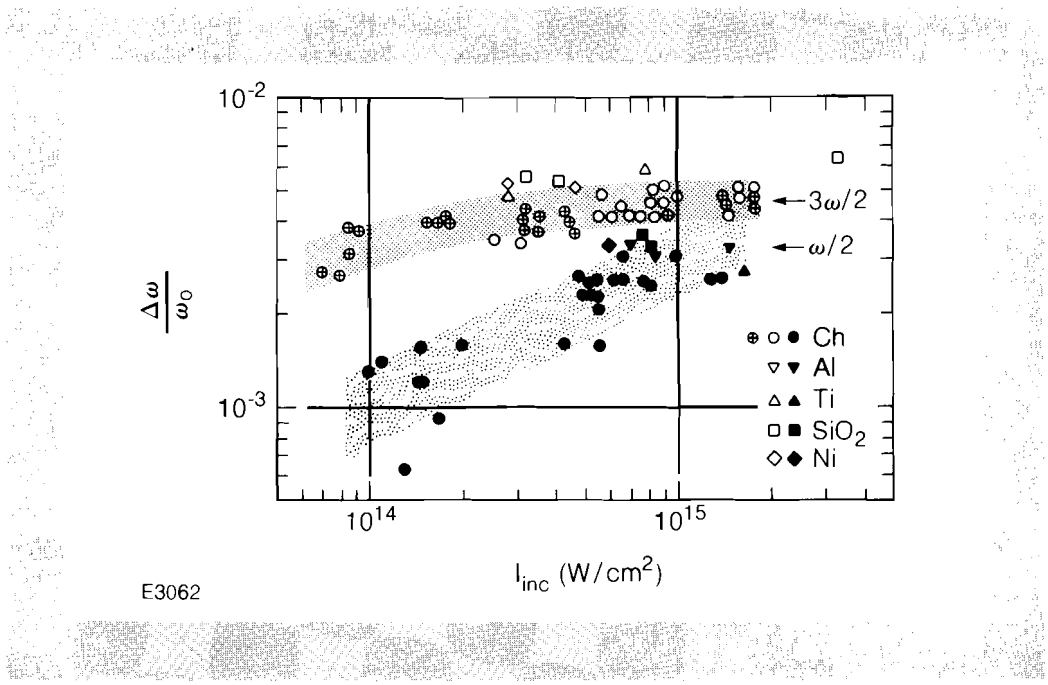

Fig. 19.10
Normalized frequency shift of the sharp red feature of the $\omega/2$ spectra and half of the spectral splitting of the $3\omega/2$ emission under uniform six-beam illumination. For the $3\omega/2$-data results from IR (1.05 μm) and UV (0.35 μm, o and other open symbols) irradiation, experiments are plotted together as the results are virtually indistinguishable. If the two harmonic generation processes were to sample the same plasmons, the two sets of data would lie on top of each other.

ACKNOWLEDGMENT

This work was supported by the U.S. Department of Energy Office of Inertial Fusion under contract number DE-AC08-80DP40124 and by the Laser Fusion Feasibility Project at the Laboratory for Laser Energetics which has the following sponsors: Empire State Electric Energy Research Corporation, General Electric Company, New York State Energy Research and Development Authority, Northeast Utilities Service Company, Southern California Edison Company, The Standard Oil Company, and University of Rochester. Such support does not imply endorsement of the content by any of the above parties.

REFERENCES

1. A. Caruso *et al.*, *Phys. Lett.* **33A**, 29 (1970).
2. A. I. Avrov *et al.*, *Sov. Phys. JETP* **45**, 507 (1977); V. Yu. Bychenkov, V. P. Silin, and V. T. Tikhonchuk, *Sov. J. Plasma Phys.* **3**, 730 (1977); A. N. Starodub and M. V. Filippov, *Sov. J. Plasma Phys.* **5**, 610 (1979); H. C. Barr, Rutherford Laboratory Annual Report No. RL-79-036 (1979), Sec. 8.3.3 (unpublished); V. V. Aleksandrov *et al.*, *JETP Lett.* **37**, 81 (1983); V. Yu. Bychenkov, A. A. Zozulja, V. P. Silin, and V. T. Tichonchuk, *Beitr. Plasmaphys.* **23**, 331 (1983).
3. R. W. Short, W. Seka, K. Tanaka, and E. A. Williams, *Phys. Rev. Lett.* **52**, 1496 (1984).
4. L. V. Powers and R. J. Schroeder, *Phys. Rev.* **A29**, 2298 (1984).
5. LLE Review **14**, 18 (1983).